Tunnelling and Underground Space Technology 83 (2019) 153–164

Contents lists available at ScienceDirect

Tunnelling and Underground Space Technology

journal homepage: www.elsevier.com/locate/tust

Three-dimensional numerical back-analysis of a monitored deep excavation retained by strutted diaphragm walls

Mohamed Nabil Houhou[a,*], Fabrice Emeriault[b], Abderahim Belounar[a]

[a] Department of Civil Engineering, Mohamed Khider University, LMN2I2S Lab, Biskra 07000, Algeria
[b] Grenoble-INP, UJF-Grenoble 1, CNRS UMR 5521, 3SR Lab, Grenoble F-38041, France

ARTICLE INFO

Keywords:
Deep excavation
Diaphragm wall
Dewatering
Numerical simulation
Settlement
Strut

ABSTRACT

The urban development often requires the use of the underground space and the number of deep excavation pits in city centers is increasing every year. To minimize the effects of excavations on adjacent structures, it is becoming increasingly important to estimate not only the lateral displacement of retaining walls but also the movement of the retained soil. Empirical methods have been developed on the basis of experimental data as to define the displacements field induced by excavation in greenfield hypothesis. However, numerical analyses can be used when more complex situations have to be analyzed. A case study of interaction between a monitored deep excavation and existing buildings is presented in this paper. The Saint-Agne subway station of Toulouse (France) new line B has been realized with a diaphragm wall supported by up to three levels of steel struts and has been built in an overconsolidated molassic geological context. The set of measurements obtained with different monitoring devices have been compared with the 3D numerical analysis using a finite difference code in which the dewatering is taken into account through an uncoupled flow-mechanical calculation. A good agreement is observed between the numerical results and the monitoring data. The model also gives an insight on the 3D behaviour of the excavation and its impact on nearby structures. Short remarks regarding the prediction of the excavation behavior by means of 2D compared to 3D numerical analysis results are briefly issued.

1. Introduction

In recent years, an increasing number of excavation works have come close to adjacent structures. Controlling ground surface deformations (both horizontal and vertical) around the excavation zone is an essential task in the design of a deep excavation. The range of these deformations is related to a complex phenomenon which depends primarily on the geological conditions, structural characteristics, construction sequences and the excavation geometry. In urban areas, excessive ground settlements frequently damage the surrounding structures (Wang et al., 2010, Ou et al., 2000).

The estimation of the ground surface displacements induced by deep excavation has been the topic of continuous research effort. One can refer to the work of Briaud et al. (2000), Clough and O'Rourke (1990), Long (2001), Moormann (2004), Ou et al. (1993), or Peck (1969). The analysis is generally based on a large number of case histories which give the relationship between the above- mentioned factors and wall deformation or ground surface settlement in greenfield conditions. This is clearly an overestimation of damage because the structure stiffness modifies the behavior of ground movements (Hong et al., 2015, Capraru and Adam, 2014, Caudron, 2007, Son and Cording, 2005). However in congested sites, soil-structure interaction phenomena occurring between the retaining wall and the existing buildings have not received much attention.

Despite the numerous developments of specific numerical codes and their encouraging results, discrepancies are still observed during comparison of numerical simulation of such structures with monitored sites (Ghareh and Saidi, 2011, Schweiger, 2008, Shao and Macari, 2008). On the other side, very limited field data are found for the response of adjacent buildings.

In this context, this research focuses on the 3D numerical modeling of an irregularly-shaped monitored deep excavation consisting of a diaphragm wall supported by several rows of steel struts. The Saint-Agne station is located on the Toulouse (France) subway line B and has been built in an overconsolidated molassic geological context with in particular a high value of K_0. The limitation of the impact of the excavation on existing buildings is a key issue because in most cases the stations are close to old buildings.

The partners of the research project METROTOUL have been given the opportunity to install on this station a complete set of measuring

* Corresponding author at: Department of Civil Engineering, Mohamed Khider University, BP 145 RP, Biskra 07000, Algeria.
E-mail address: nabil.houhou@univ-biskra.dz (M.N. Houhou).

https://doi.org/10.1016/j.tust.2018.09.013
Received 20 April 2018; Received in revised form 5 August 2018; Accepted 26 September 2018
Available online 09 October 2018
0886-7798/

devices. Two particular sections have been studied in further details to improve the understanding of ground response and the soil-structure interaction phenomena induced by deep excavation close to existing buildings and to collect precise data for validating numerical models. The basement was completed using semi top-down construction. The whole construction activities include staged dewatering, excavation and strutting.

The aim of the present paper is to performed a full numerical back-analysis of the behaviour of the excavation in terms of lateral displacements of diaphragm walls, ground surface movements, and internal forces in struts, as well as the impact on the existing buildings and to shed some light on the 3D nature of the movements induced by the excavation.

The FLAC^{3D} software (Itasca, 2012) is used to model the various phases of the work. All the parameters come either from standard laboratory tests or from previous back-analysis in similar location and on similar underground works. The only “adjusted” parameter concerns the effective stiffness of the steel struts that is back-calculated from measured strut loads and associated wall deformation (that implicitly account for the installation conditions). The results of this 3D model are validated by comparing them to the in-situ measurements. The pertinence of the 3D model is also judged by comparison with the 2D plane strain model, implemented in the FLAC^{2D} code.

2. Case study of a deep excavation

2.1. General description of the project

The Saint-Agne station is located on the new line B of Toulouse subway. This station is a 55.2 m × 17.15 m rectangular deep excavation (Fig. 1). The retaining structure consists of a cast in situ diaphragm wall with a thickness of 1.0 m. The depth of the diaphragm wall was set to about 20.65 m as presented in Fig. 2. During the excavation to a depth of 17.2 m, the retaining walls were supported at the top by partial slabs and diagonal beams and in depth by means of three levels of temporary steel struts 0.61 or 0.66 m in diameter and 10 or 12.5 mm thick as depicted in Figs. 2 and 3. A typical plan view of the wall strutting is shown in Fig. 4. This station is surrounded on the south side by residential houses R + 1, and on the North side by a building R + 0 (noted building A) which will be of particular interest afterwards and of a building R + 2 (noted building B) as presented in Fig. 1.

2.2. Construction sequences

The method of strutted diaphragm walls is one of the most commonly used methods of deep excavation support. Preexcavation of about 1.9 m depth was required for the implementation at the top of the wall of partial slabs and diagonal beams (West side).

The whole construction activities included staged dewatering, excavation and strutting. At each stage, dewatering is first performed to lower the ground water table down to 1 m below the bottom of the subsequent stage of excavation, then the soil is removed and followed by the installation of all the struts at 0.4–0.5 m above the bottom of the excavation. Step by step, the subsequent staged dewatering, excavation and strutting phases can follow each other until the final bottom of excavation is reached. Table 1 summarizes the different excavation phases and schedule.

2.3. Geological and geotechnical context

The regional geological substratum is constituted by molassic formations dating from the Tertiary. These grounds have been overtopped by a minimum of 200 m of Stampien and Miocene which have been eroded before the deposition of the quaternary alluviums. In fact, the Toulouse molasses exhibit a very high overconsolidated behavior with in particular a high value of the at rest earth pressure coefficient K_0.

For the preliminary geological survey, several boreholes were drilled within the station area. It can be noted that the site shows a very heterogeneous lithological structure. The molasse is either clayey or sandy, the layers alternate in depth. Over the whole height of the excavation, there are mainly compact clayey sandy molasses with some thin interbedded sandy layers. The molasse is overlain by 1.2 m of fill and alluvial sandy silt and the water table is approximately 2 m below the ground level. A preliminary hydrogeological study has highlighted the risk of raising the water table due to its partial cut by the diaphragm walls. As a result, the retaining wall was designed with a reduced embedded length.

In order to determine deformation moduli in the range of the stresses which reign in the soil mass, high pressure CD triaxial tests (300 kPa to 3 MPa) were carried out on different soil samples (Serratrice 2005). A clear dependence of the moduli with the confining stress is observed. Given all the tests carried out and the dispersion of Young's modulus values, a linear increase of this module with depth z is proposed (it does not take into account the lithologic distinction between clayey molasses and sandy molasses but considers the molassic substratum as homogeneous in terms of deformability):

$$E(MPa) = E_0 + \beta . z = 66 + 9,9 . z(m) \quad (1)$$

This linear variation is also based on the numerical back-analysis of the excavation of a 8.0 m in diameter tunnel in the vicinity of the project (Houhou et al., 2016) and of the Jeanne d’Arc deep excavation, a similar work whose characteristics are substantially equivalent and realized in the same geological context (Houhou et al., 2010).

High pressure K_o oedometer tests (Serratrice, 2005) revealed that the molasses are overconsolidated and have a transition to a normally consolidated behaviour for stresses of about 2 MPa. Preconsolidation stress is therefore estimated close to 2 MPa (in agreement with the geological analysis mentioned above). These tests have also shown that the overconsolidated molasses is subject in-situ to very high horizontal initial stress (K_o is estimated equal to 1.6). The main geotechnical characteristics of molasses deduced from laboratory tests are presented in Table 2.

2.4. Description of the monitoring sections

Two fully equipped monitoring sections have been installed on the Saint-Agne excavation site (Fig. 1): Section 2 corresponds to Greenfield conditions whereas Section 1 includes a 9 m × 27 m old brick building perpendicular to the excavation with a minimum distance to the diaphragm wall equal to 2 m. Each section includes one inclinometer in the diaphragm wall, 4 vibrating wire strain gauges (Type SC-5 E Telemac) installed at mid-span on each of the three strut levels with automatic data acquisition and precise levelling. Horizontal extension of the brick building is measured on several intervals with Distomatic invar thread as well as crack opening with Demec strain gauges.

The data collected during all the construction phases (excavation, strut installation, slab concreting and strut removing) are further presented and analysed. The comparison of the results obtained for Sections 1 and 2 gives an insight on the soil-structure interaction phenomena induced by deep excavation close to existing buildings.

2.5. Analysis of monitoring results

2.5.1. Deflection of the diaphragm wall

The diaphragm wall deflections are measured by the two inclinometers I_1 and I_2. Measurements are performed in both transverse and longitudinal directions. Thus, the movements of the diaphragm wall may be obtained in both directions at each phase of work. The movements in the transverse direction (perpendicular to the long side) are greater than in the longitudinal direction. The measurements show that the deformed inclinometer tubes 1 and 2 resulting in the longitudinal direction, remain within the range of measurement accuracy

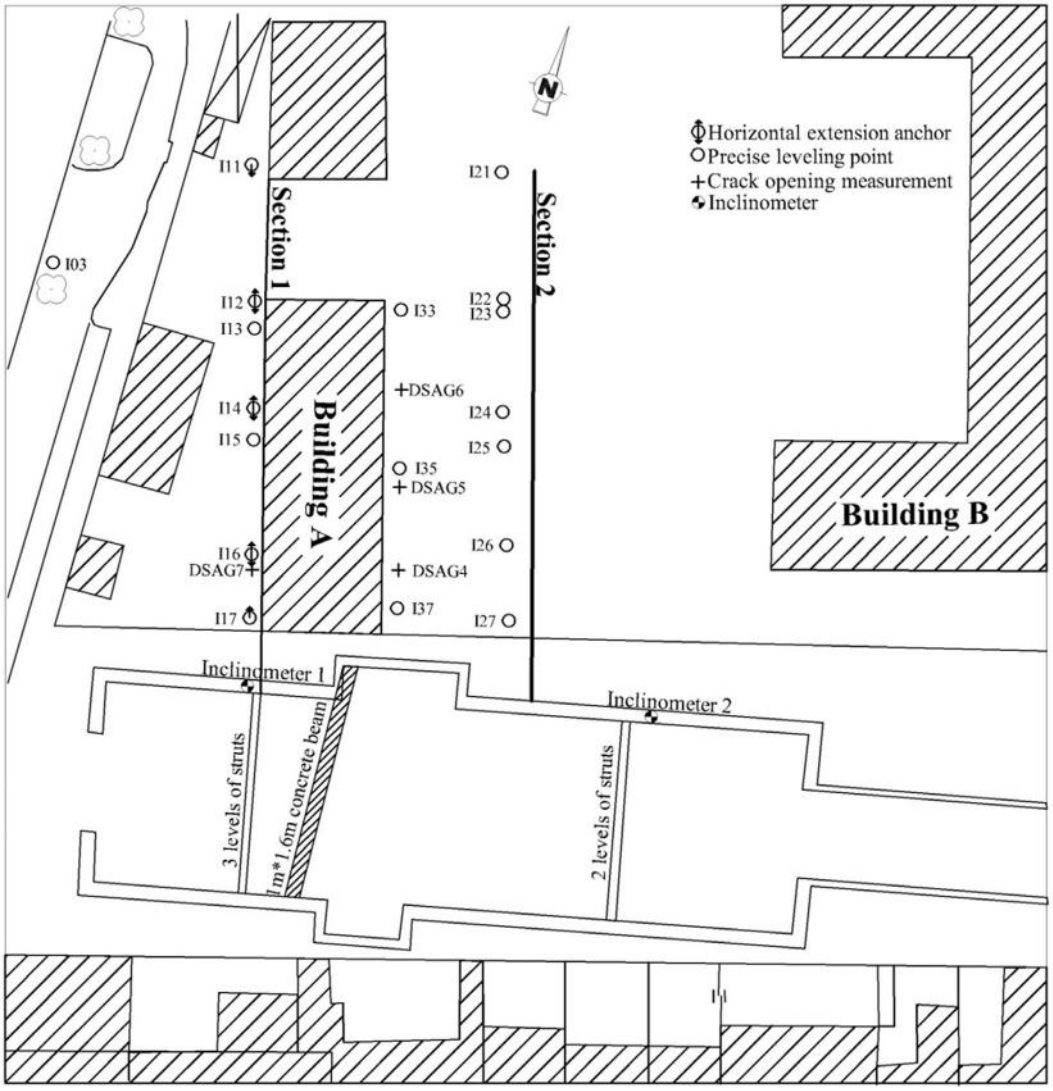

Fig. 1. Global view of the site and location of the instrumentation.

(± 1 mm), which allows to consider that there is no real movement of the wall in this direction.

Figs. 5 and 6 present the horizontal displacement profiles obtained in inclinometers 1 and 2 respectively. A lack of grouting in the upper part of the inclinometer casings leads to discard all the values measured for the first 3 m. Nevertheless, it appears that the movements obtained are very similar in shape and amplitude; at the final excavation phase the displacements being slightly greater in the case of I_1 (δ_{hmax} is close to 8.6 mm instead of 7.7 mm for I_2). The maximum lateral wall displacement δ_{hmax} represents 0.05% of the excavation depth H. This value corresponds to low values with respect to the range reported by Clough and O'Rourke (1990), Leung and Ng (2007) or Moormann (2004) for similar cases of excavation (δ_{hmax} ranges from 0.15 to 0.2% H). This low value can be due to the larger stiffness of the diaphragm wall (compared to other retaining wall types recorded in databases). In the upper part of the diaphragm wall, a partial concrete slab (0.4 m thick) and a concrete beam (1.6 m high and 1 m thick) induce in the vicinity of Inclinometer 1 an increase in stiffness (cf. Fig. 1). This explains that the behaviour of the top part of wall is mainly rotational whereas for the Inclinometer 2, the observed movement corresponds to a deflection towards the centre of the excavation.

Because the final embedded length of the wall is rather small (3.45 m), a global rotation movement is observed in the lower part of the wall and in the soil 2 m beneath the tip of the wall.

Figs. 5 and 6 also present the displacement profiles obtained after the construction of the base slab and the removal of the lower level of struts. The maximum induced horizontal movements are close to 1 mm.

2.5.2. Struts load

In total, five struts were instrumented. For Section 1, the strut loads are monitored in the three levels of steel struts denoted 1-1 (upper), 2-1 (middle) and 3-1 (bottom). It is reminded that a 1 m × 1.6 m concrete beam is constructed across the excavation at the top of the wall and that the load carried by this beam is not measured. For Section 2, only two levels of struts are used (denoted 2-2 and 3-2), since a partial concrete slab was implemented at the top of the wall at the end of phase 3.

On each of the steel cylindrical struts, four vibrating wire strain gauges are installed at mid-span at 0°, 90°, 180° and 270°. Therefore, the axial force and bending moments in the vertical and horizontal plane can be calculated. In this paper, only the axial force will be considered.

Figs. 7 and 8 show that the different excavation phases lead to a gradual increase in struts load (with a stable value obtained within a week after the excavation). Due to the period in which most of the excavation has been performed (summertime), the struts are subjected to thermal dilation/shortening due to the daily cycles of temperature. This effect is even larger in case where the struts are exposed to the direct radiative effect of sun light. In particular this effect is larger for

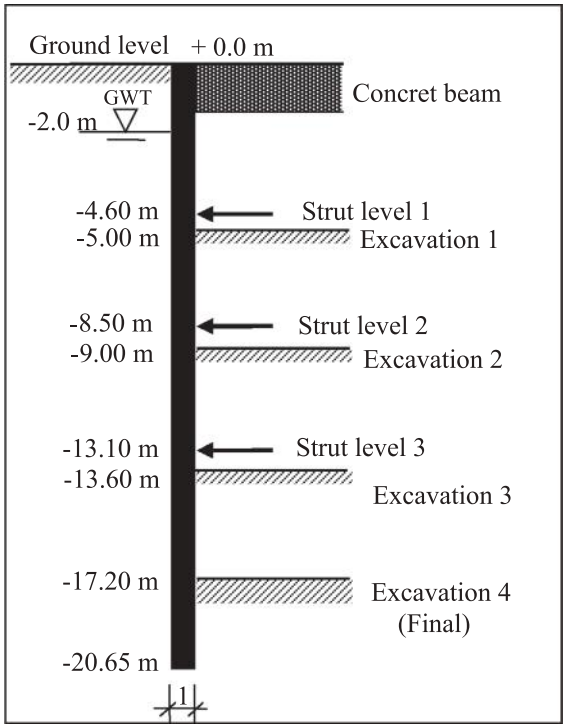

Fig. 2. Cross-section of the diaphragm wall (section 1).

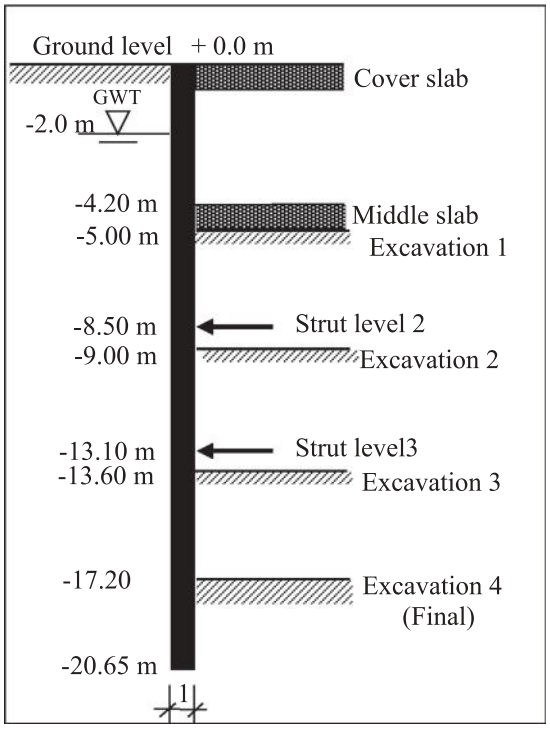

Fig. 3. Cross-section of the diaphragm wall (section 2).

the upper row of struts. It can be seen from Figs. 7 and 8 that the daily variations of axial load in the struts induced by this phenomenon can range from 50 to 200 kN according to the period.

Although the measurement period for the lower strut 3-1 is relatively short, the axial force evolution during excavation phases is much more pronounced (Fig. 8). The load carried by Strut 1-1 are not presented because they remain relatively small (less than 500 kN) throughout the different excavation phases.

Fig. 9 summarizes the measured strut loads at the end of Phases 4, 6 and 7 and two weeks after the completion of the excavation works. The chosen dates correspond to (a) stabilized values of the load and (b) to dates of inclinometric surveys. From the horizontal movement profiles, one can infer the global shortening δ of the different struts. Assuming that δ is only due to variation of axial force in the strut (bending is neglected), the induced load can be calculated from δ and the nominal characteristics of the strut (length 2*L*, section *S* and Young's modulus of steel $E = 210$ GPa) by:

$$F = \delta \frac{SE}{L} \tag{2}$$

Fig. 10 presents the results obtained for Struts 1-1 to 3-1. An efficiency coefficient smaller than 1 has been introduced in the analysis to represent the non-linearity of the elastic characteristics of the steel and strut-wall contact. The strut load is thus calculated with:

$$F = \delta \frac{SE}{L} c_{eff} \tag{3}$$

In Fig. 10, a 50% efficiency coefficient has been chosen. It appears that the calculated values are in good agreement with the measured ones for the three struts and the different excavation phases.

2.5.3. Greenfield settlements

Vertical displacements at surface points are the result of movements induced at larger depths, which propagate upwards. Schematically, the main causes of vertical settlements at the ground surface can be assumed to be (a) the horizontal movements of the retaining structures; and (b) the stress relief associated to the excavation, induced heave of the soils located below the bottom of the excavation.

For Section 2, precise levelling of 7 points (labelled I_{21} to I_{27} – see Fig. 1) is performed at each step of the excavation. Fig. 11 shows that the obtained settlement profiles are of the spandrel type. At the end of the excavation phases, a maximum settlement of 3.5 mm is obtained close to the top of the wall and at a distance of 40 m this settlement is only reduced to 1.5 mm.

In this case the normalized maximum ground settlements δ_{vmax}/H is approximately equal to 0.023%, which is very small compared to the average values of 0.15% reported by Clough and O'Rourke (1990), Moormann (2004), Leung and Ng (2007) and Capraru and Adam (2014) for stiff clays. This result can be partly explained by the high shear strength of the molasses and the rigidity of the 1 m thick diaphragm wall.

A settlement influence zone can be estimated at 63 m, i.e. 3.7*H*, which is greater than all the values reported by Peck (1969), Clough and O'Rourke (1990) or Hsieh and Ou (1998). The high K_0 value exhibited by the molasses (close to 1.6) can be responsible for this larger than usual extend of the excavation influence zone. Emeriault et al. (2008) and Houhou et al. (2016) have shown that this high K_0 is also responsible for horizontal movements larger than expected on several monitoring sections of tunnel and galleries of the subway line B.

Fig. 11 also proves that the final settlement trough is quickly obtained at the end of the excavation phases: the trough measured after 5 months only departs from that observed at the end of final excavation (phase 7) by 0.35 mm.

2.5.4. Soil-structure interaction

During the excavation, the settlements and horizontal deformations as well as the cracks opening are measured in the one-storey brick Building A (Section 1, cf. Fig. 1).

2.5.4.1. Building settlements. During the first excavation phases, the settlement troughs observed on the west side of the instrumented building (Fig. 12) are very different from those obtained in greenfield conditions. It appears that the amplitude of settlements is reduced; a maximum value of 1.65 mm is obtained close to the top of the

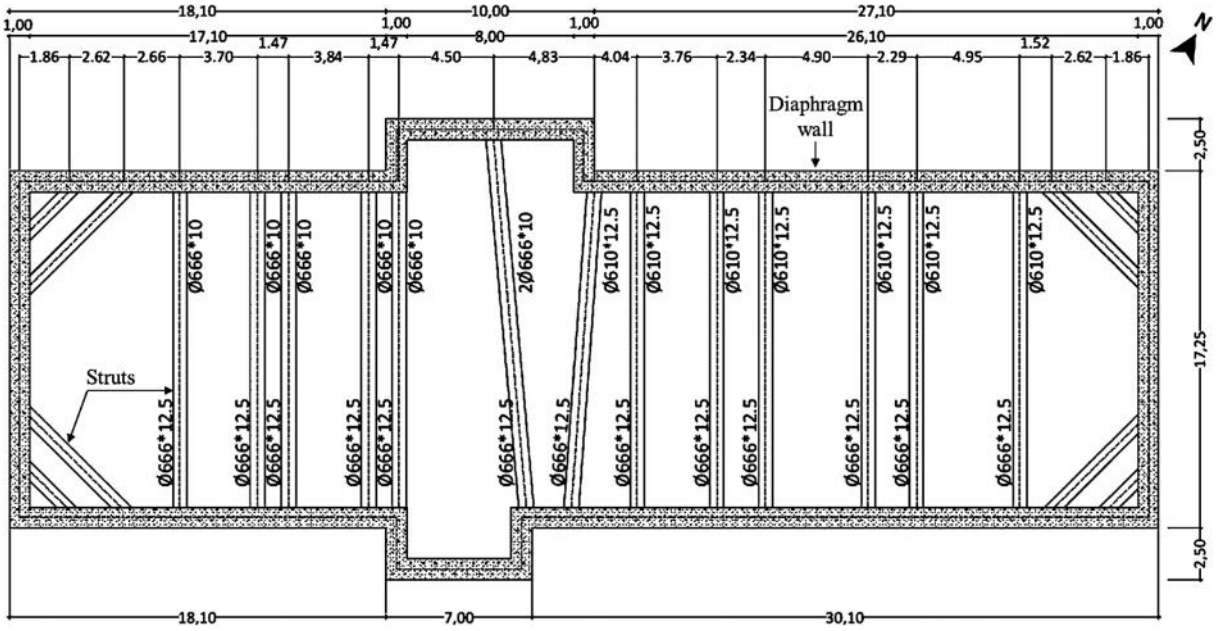

Fig. 4. Plan view of the excavation at level −8.5 m and −13.1 m.

Table 1
Construction phases.

Phase	Activity	Date	Level (m)
0	Preexcavation	07/04-02/06/03	−1.9
	Partial concrete slabs and Beams (West side)		+0.0
1	Excavation 1	05/06-18/06/03	−5.0
2	Cover and Middle slabs (East side)	19/06-07/07/03	+0.0
			−4.20
	Installation of strut 1 (West side)	23/06-02/07/03	−4.6
3	Excavation 2	30/06-11/07/03	−9.0
4	Installation of strut 2	01/09-12/09/03	−8.5
5	Excavation 3	12/09-01/10/03	−13.6
6	Installation of strut 3	13/10-21/10/03	−13.1
7	Excavation 4	30/10-28/11/03	−17.2
8	Base slab (invert)	3/12-03/02/04	−16.85
	Removing of strut 3	23/01-03/02/04	−13.1

diaphragm wall at Phase 5. Besides, the shape does not correspond to the spandrel type. Due to technical problems, the settlement trough at the end of Phase 7 (final excavation) is not complete. Nevertheless,

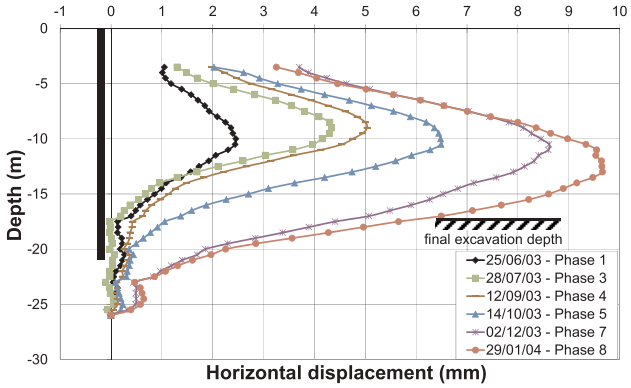

Fig. 5. Horizontal displacements measured in Inclinometer 1.

after 5 months, the settlements close to the wall are almost equal to those measured in Greenfield conditions. The main difference then lies in the extent of the trough: for Section 1, significant settlements are only measured below the brick building with a quasi linear evolution.

From Fig. 13, the settlement troughs observed for the eastern facade of the building seem to correspond to a smooth transition between the results of Sections 1 and 2. The maximum vertical displacement is not influenced by the presence of the light brick building, the building (and its horizontal stiffness) only affecting the width of the settlement trough. Moreover, the global stiffness of the diaphragm wall seems to be equivalent in the two cases even though:

Table 2
Summary of main geotechnical properties of soil stratigraphy.

Soil type	Depth (m)	γ (kN/m^3)	K (m/s)	K_0 (–)	ν (–)	c' (kPa)	φ' (°)	Ψ (°)	c_u (kPa)	φ_u (°)	E (MPa)	UCS (MPa)
Fill/alluvium	0–1.2	20	6.10^{-4}	0.5	0.3	0.0	25	0.0	0.0	25	66–78	N/A
Clays	1.2–2.8	22	1.10^{-9}	1.6	0.3	80	33	0.0	300	24	78–94	0.75
Clay sands	2.8–5.2	21	1.10^{-7}	1.6	0.3	52	37	3.0	120	33	94–117	0.18
Sandy clays	5.2–7.6	22	5.10^{-8}	1.6	0.3	84	32	0.0	210	18	117–141	0.54
Fine to medium sands	7.6–8.6	21	1.10^{-6}	1.6	0.3	0.0	36	5.0	0.1	35	141–151	N/A
Sandy clays	8.6–10.2	22	5.10^{-8}	1.6	0.3	84	32	0.0	210	18	151–167	0.54
Fine to medium sands	10.2–12.7	21	1.10^{-6}	1.6	0.3	0.0	36	5.0	0.1	35	167–191	N/A
Sandy clays	12.7–21	22	5.10^{-8}	1.6	0.3	84	32	0.0	210	18	191–274	0.54
Clays	> 21	22	1.10^{-9}	1.6	0.3	80	33	0.0	300	24	274–360	0.75

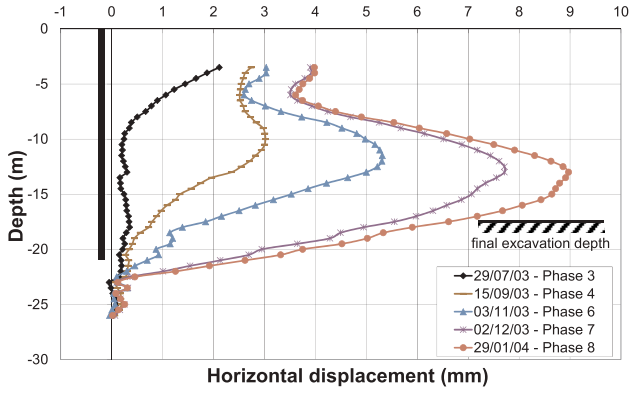

Fig. 6. Horizontal displacements measured in Inclinometer 2.

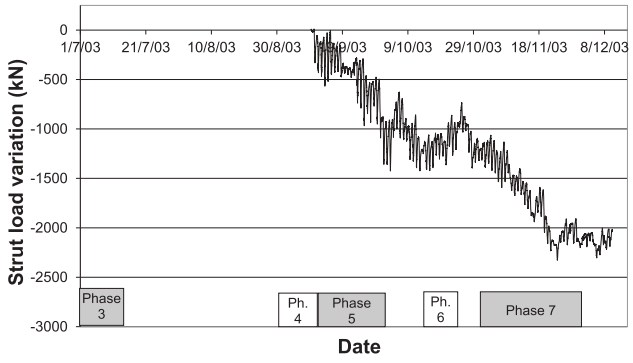

Fig. 7. Normal force in strut 2-1.

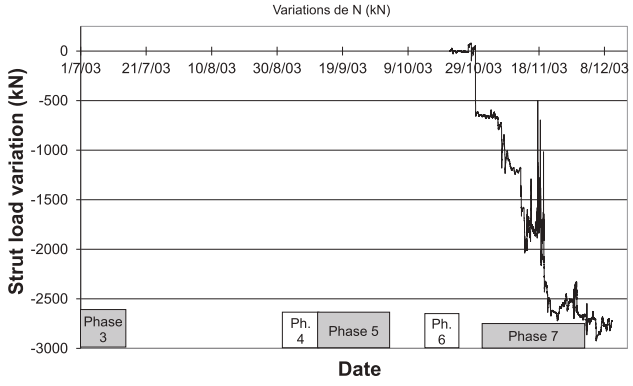

Fig. 8. Normal force in strut 3-1.

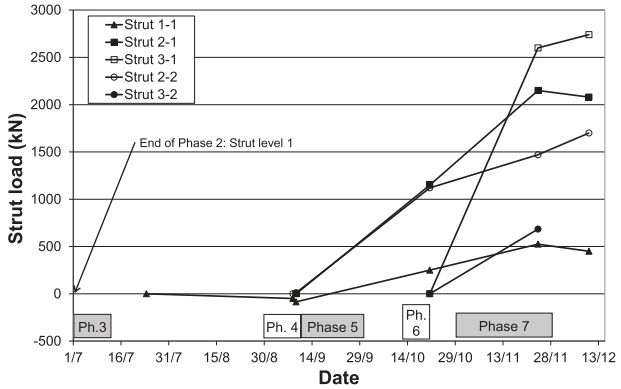

Fig. 9. Axial force in the different monitored struts.

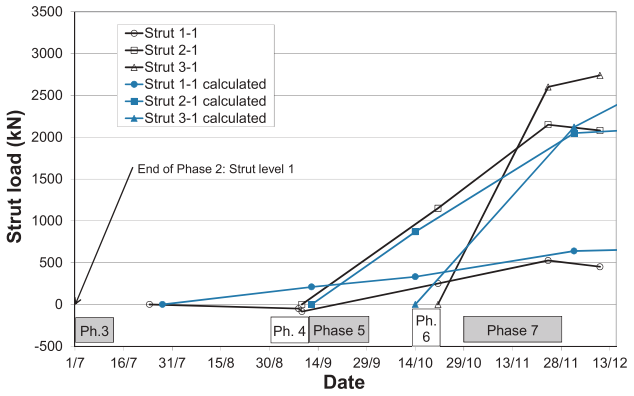

Fig. 10. Comparison of calculated (based on the inclinometer measurements) and measured axial forces in struts 1-1 to 3-1 – An efficiency coefficient equal to 0.5 is used in this figure.

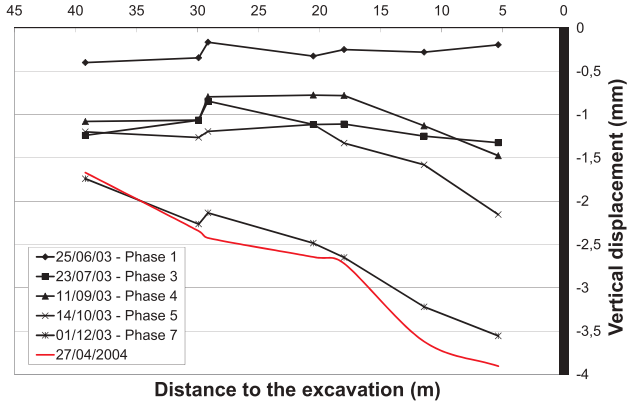

Fig. 11. Greenfield settlement trough (points I_{21} to I_{27}).

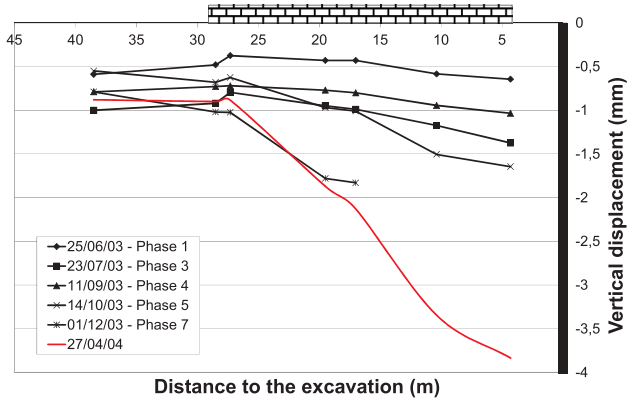

Fig. 12. Settlement trough observed on the west side of the building *A* (points I_{11} to I_{17}).

- For Section 1, the large concrete beam reduces the possible deflection of the wall
- For Section 2, the irregular shape of the diaphragm wall increases its stiffness.

2.5.4.2. Horizontal deformations. Horizontal deformations are measured between several anchors installed on the west facade of Building A (points I_{12}, I_{14}, I_{16} and I_{17}, see Fig. 1). The results obtained for interval I_{14}-I_{16} and I_{16}-I_{17} are also checked by the measure of the total extension of interval I_{14}-I_{17}. Finally, points I_{11} and I_{12} are located on two separate buildings and therefore the measure gives the relative displacement of the two structures.

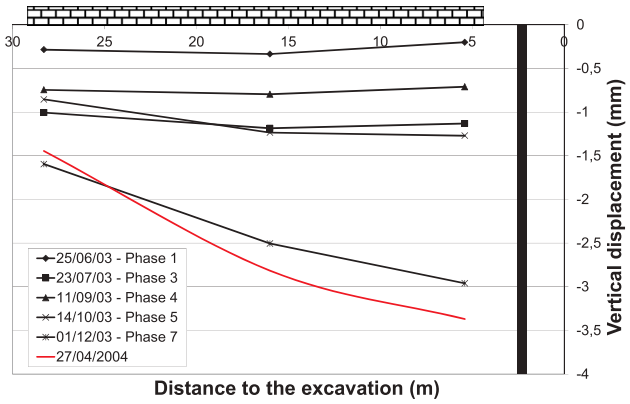

Fig. 13. Settlement trough observed on the east side of the building *A* (points I_{33} to I_{37}).

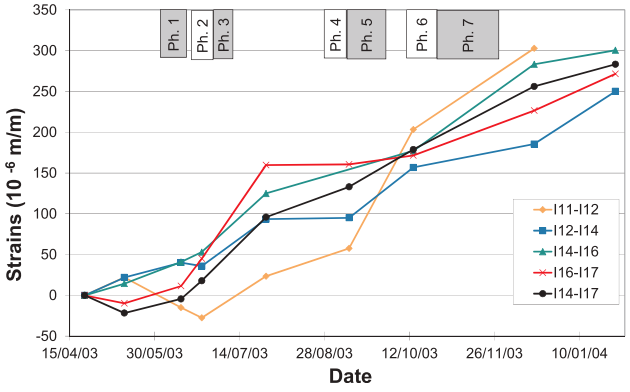

Fig. 14. Horizontal extension of the building *A*.

Fig. 14 shows that at the end of Phase 8 (2 months after completion of Phase 7), the extensions measured for the different intervals are very close (approximately 0.03%), indicating that a global linear horizontal displacement profile is observed in addition to the linear settlement profile of the structure (cf. Fig. 12).

Nevertheless, during the four excavation phases, the extensions are not uniformly distributed along the structure. Actually, it is only at the end of Phase 4 that the distance between points I_{11} and I_{12} increases, indicating a horizontal movement of I_{12} towards the excavation while I_{11} remains still.

2.5.4.3. Crack opening. Demec strain gauges are also used to determine existing crack opening in the Building A. The four cracks that have been equipped (denoted DSAG4 to DSAG7, cf. Fig. 1) have an initial width ranging from 0.5 to 1 mm. Fig. 15 presents the results obtained for DSAG7 and DSAG4 located at the bottom of the western and eastern facade of Building A, respectively (Fig. 1). For DSAG7 the observed movements correspond to a global increase of the crack width of approximately 0.9 mm at the end of the excavation phases. The increase of the distance in Direction 1 is slightly greater than that in the Direction 2. This indicates that in addition to the extension of the crack in the normal direction, it also exhibits a hogging tendency. Opposite results are obtained for DSAG4 (with an average crack opening of 0.2 mm) indicating a tendency to sagging. On the whole, there seems to be a twisting movement induced by the differential settlement troughs on either side of the building. However, for the DSAG5 and DSAG6 cracks, we do not observe any significant movement (crack width less than 50 μm). DSAG5 and DSAG6 remain unaffected by the structure settlements and horizontal displacements.

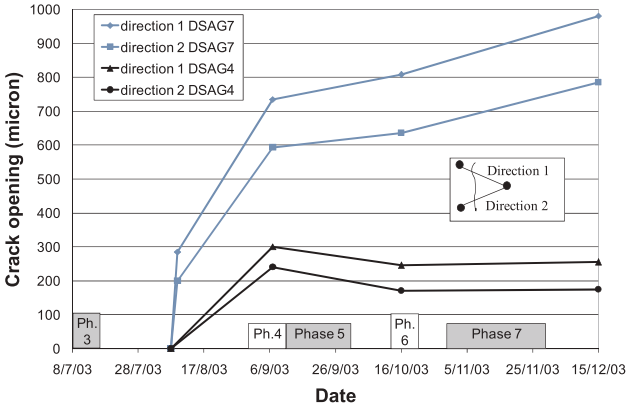

Fig. 15. Crack opening measurements (DSAG4 & DSAG7).

3. Three-dimensional numerical modeling

3.1. Construction of the model

Given the irregular shape of the diaphragm walls and the complexity of the realization phasing, the behavior of the deep excavation and surrounding soil presents a particularly marked three-dimensional character. The finite difference formulation with the numerical code FLAC^{3D} (Itasca, 2012) was designed to simulate the various phases of excavation such as dewatering, soil excavation process, strut installation, slab concreting, ….

In order to minimize border effects on the behavior of the ground near the walls, the mesh extends laterally 50 m away from the walls and vertically 35 m below ground level (the bottom of the mesh is best placed at a depth where soil becomes notably harder). All nodes on the vertical sides of the model are restrained from moving in the horizontal direction and all nodes on the bottom surface are restrained in both horizontal and vertical directions. These boundaries are supposed to be impervious. The level of the water table is maintained constant 2 m below ground level outside the walls. The level inside is supposed to be horizontal and modified at each stage of dewatering (which means that the water, inside the excavated area, is assumed to be pumped). A part of the grid at the final excavation phase is shown in Fig. 16. Sensitivity analysis of the mesh density shows that it is necessary to have a refined mesh in zones close to the diaphragm walls. In the distant zones, it is possible to enlarge the mesh in order to reduce computation time.

To model the behavior of the soil, a linear elastic perfectly plastic constitutive law with a Mohr-Coulomb yield surface and plastic potential was used in this study. A non-associated condition in which the plastic potential is defined by an angle of dilation was adopted. This choice is justified by the highly overconsolidated character of the

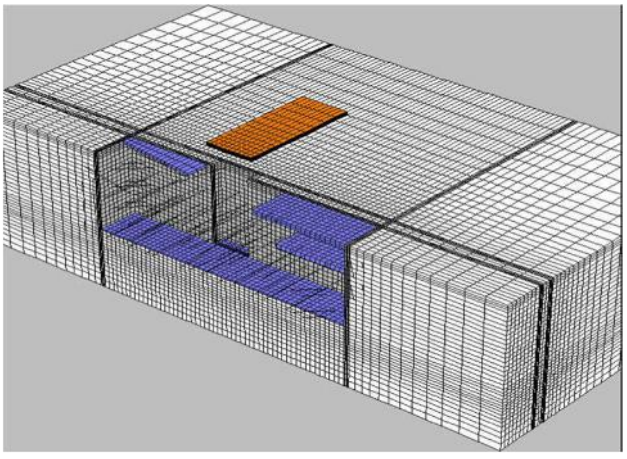

Fig. 16. FLAC^{3D} grid.

molasses (K_0 = 1.6). This one leads during the different phases of excavation to a substantially elastic behavior of the soil as well in zones in load as in those subjected to unloading. The Mohr–Coulomb model has the advantage of requiring few soil parameters and that all these parameters can be determined from the conventional soil tests performed for this construction project. The use of a more sophisticated constitutive model will probably necessitate the evaluation of specific soil parameters from special tests. Consequently the number of material parameters to be identified would be greater, and their interdependence is not obvious.

The geotechnical parameters retained for the different layers in the numerical model are summarized in Table 2. A linear variation of Young's modulus of the soil with depth is proposed in the numerical simulation (see Eq. (1)).

The diaphragm wall is discontinuous in the horizontal direction along the sides of the excavation because it is constructed by sections of wall panels and starter bars were not used to provide moment connections between adjacent panels. Consequently, it cannot sustain any significant out-of-plane bending, and the horizontal stiffness of the wall is also much smaller than the stiffness of the solid concrete, as a consequence of vertical joints between the different panels. Hence, it is necessary to reduce the out-of-plane wall stiffness (both axial and bending) to an appropriate value, if reasonable predictions of wall and ground movements and structural forces are to be obtained when modelling full 3D excavations.

Thus, in the current case study, the diaphragm wall was modelled using anisotropic linear elastic solid elements. The Young's modulus of the diaphragm wall was taken as 30 GPa. The horizontal stiffness of the wall (E2) was assumed to be 100 times less stiff than the solid concrete stiffness (E1) or E_2/E_1 ratio of 0.01 to account for the lack of continuity in diaphragm wall in the horizontal direction (along its longer side) as suggested by Zdravkovic et al. (2005). The contact between the diaphragm wall and the soil was set to be rigid. It has been verified that this assumption does not induce any development of plastic zones in the soil elements in contact with the wall. To characterize the interaction between wall and slabs the ATTACH command was applied. This command is used to connect adjoining primitive shapes with different zone sizes and therefore forms an unbroken continuum. The ratio of zone sizes must be adjusted to ensure continuities in the displacement and stress distribution across the attached grids. The passive strut (circular steel tube) is normally subjected to axial loads; therefore one-dimensional isotropic linear elastic model was used to simulate struts, with a Young's modulus of 210 GPa for the steel. As for the wall–struts interaction, the connection between the diaphragm wall and the struts was hinged in order to avoid the transmission of bending moments. This is accomplished by slaving the strut node to the horizontal displacements of the walls. With this procedure, the wall and the strut can move without causing any moment between them. The fine analysis of the results provided by the instrumentation of the walls and struts showed that the simultaneous evolution of the global shortening of the different struts and the strut loads can be explained only with a reduction factor of 2 on the struts theoretical stiffness (see Section 2.5.2). However, due to this difference between theoretical and effective stiffness (usually observed in practice), the later was considered equal to half the theoretical stiffness. Structural elements properties used in the numerical analysis are summarized in Table 3.

The existing buildings on the south side were simulated by a uniformly distributed load of 15 kPa (this is a rough estimate, considering the self-weight and overhead of a residential buildings R + 1). However, building *A* (cf. Fig. 1) is modeled by volume elements linked to the mesh by interface elements having an elastoplastic behavior with a Coulomb shear-strength criterion (Itasca, 2012, Franzius et al. 2006). Detachment was made impossible by adjusting the separation failure criterion to an extremely important value (tensile strength = 10^{10} Pa). The used interface is characterized by a friction angle equal to the friction angle of the soil φ, zero cohesion, a normal stiffness $K_n = 2.10^{10}$ Pa/m and a shear stiffness $K_s = K_n$. The properties of this interface are chosen so as to simulate a rigid contact between the soil and the building. The system of shallow foundations was not explicitly represented.

In order to compare accurately the numerical modeling results with the in situ measurements, the chronology of the measurements was studied in order to determine which measurements correspond more to a particular phase of the numerical modeling. The results of this analysis are shown in Table 4. Thus, the full construction is simulated by a series of seven successive calculation steps. The analyses assumed that the diaphragm wall was "wished-in-place" and hence, did not consider local changes in stresses or soil properties associated with trench excavation and concreting. During excavations, the ground water table is lowered down to 1 m below the bottom of each excavation.

To model the effect of successive lowering of the water table an uncoupled flow-mechanical calculation process has been performed. The analysis was carried out in two stages. The new pore pressures distribution, induced by the dewatering, was obtained primarily by a flow calculation not coupled to the mechanical behavior (using a flow-only simulation). The flow effect, induced by the dewatering, on the soil-wall mechanical behavior is then obtained simply by imposing the pore pressure thus obtained at any point of the mesh. This second analysis step was performed by a mechanical computation not coupled to the flow (by setting flow off and set the water bulk modulus to zero for this mechanical-only calculation). In this way the pore pressure field will not be changed by the volumetric strain. This is the long-term behavior.

3.2. Behavior of the diaphragm wall

Fig. 17 shows the variation of maximum lateral wall deflection along the wall for each stage of excavation. The corresponding results for the final stage of excavation using the two-dimensional analysis are also indicated in the figure (horizontal dotted line). It can be seen from Fig. 17 that the maximum horizontal displacements (δ_{hm}) present a strong variation along the wall, which reflects well the corner stiffening effects (soil arching around corners) already mentioned by Houhou et al. (2010), Lin et al. (2003) and Finno et al. (2007). The results also clearly demonstrate that geometrical effect (irregular shape) has a significant impact on the induced wall deformations.

It is also noted that the displacement of the wall steadily increases with the depth of excavation. At the final stage (step 6), the displacements predicted by the 2D analysis are relatively overestimated throughout the wall. This suggests that an effect of excavation corners persists and that the plane strain conditions do not prevail even near the center of the excavation wall. Thus, it has been shown that the plane strain simulations might give conservative results especially for the center portion of the excavation. For section in corner areas, the analysis would be much more conservative because the three-dimensional effects in this region are not considered.

It should be noted that a calculation with a nominal stiffness of struts was performed and showed an underestimation of approximately 23% of the largest wall deflection and ground surface movement, while the deformation pattern is maintained.

Figs. 18 and 19 show the comparison of the 3D numerical analysis and the field measurements for inclinometers I_1 and I_2, respectively, for each stage of excavation.

According to the wall deflections profiles obtained from 3D numerical analysis, it is clear that the wall, at the location of I_2, behaves initially (after the first excavation phase) as an unanchored wall (cantilever), with a maximum displacement of 5 mm at the top, which is consistent with the fact that no support has been set up on the east side in this phase. On the other hand, on the west side at I_1 location, the preliminary installation of a transverse beam (as well as 2 partial slabs on the surface) has limited the displacements at the top. However, while the excavation progresses in depth (excavation 2, 3 and 4), the

Table 3
Structural elements properties used in numerical analysis.

Element type	γ (kN/m^3)	D (m)	t (m)	E_1 (MPa)	E_2/E_1 (–)	ν (–)	EA (MN)	EI (MN.m^2)
Diaphragm walls	25	–	1.07	30,100	0.01	0.2	–	–
Partial and base slabs	25	–	0.45	30,140	–	0.2	–	–
Middle and cover slabs	25	–	0.85	30,285	–	0.2	–	–
Diagonal beams	25	–	–	32,600	–	0.2	55,420	13,347
Struts level 1	78.5	0.61	0.010	105,000	–	0.3	1978.20	89.09
Struts level 2	78.5	0.66	0.0125	105,000	–	0.3	2669.83	139.97
Struts level 3	78.5	0.66	0.010	105,000	–	0.3	2144.10	113.26
		0.61	0.0125				2463.61	109.99

D: exterior diameter; t: thickness; EA: axial stiffness; EI: bending stiffness; ν: Poisson's ratio; A: cross-sectional area; I: second moment of inertia.

Table 4
Relationship between calculation steps and main in situ measurements.

Date	Activity	Calculation steps	Measures
	Generation of the initial stress field (K_0 procedure)	Step 0	0
07/04-02/06	Preexcavation Partial slabs and Beams (west side)	Step 1	1
05/06-18/06	Excavation 1	Step 2	2
19/06-07/07	Middle and Cover slabs (east side)		2′
23/06-02/07	Installation of Strut 1		
30/06-11/07	Excavation 2	Step 3	3
01/09-12/09	Installation of Strut 2		3′
12/09-01/10	Excavation 3	Step 4	4
13/10-21/10	Installation of Strut 3		4′
30/10-28/11	Excavation 4	Step 5	5
3/12-03/02	Bottom slab and Removing of strut 3	Step 6	6

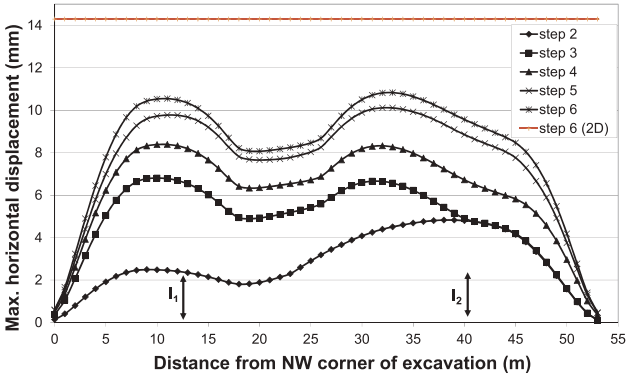

Fig. 17. Evolution of the maximal horizontal movements along the wall.

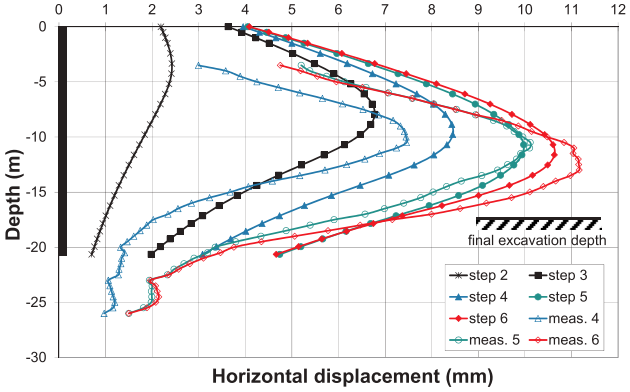

Fig. 18. Comparison of simulation and measurements of the inclinometer I_1.

wall pivots with respect to the points of high rigidity (beam and slabs). Therefore, the wall shows a displacement profile of deep inward type. It should be noted that the installation of the cover slab on the surface is an effective way to control the movement of the wall, in particular its movement at the head. The installation of the bottom slab and the

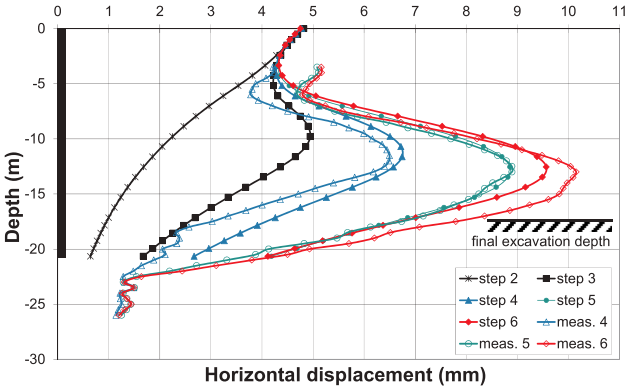

Fig. 19. Comparison of simulation and measurements of the inclinometer I_2.

simultaneous removal of the lower level of struts further increases the wall movements.

The behavior of the soil below the excavation bottom is to be taken into account. The deconfinement of the soil due to the excavation, induces a relaxation of the stresses beneath the excavated zone (reduction of the apparent weight of the soil) which causes a heave of the soil below the excavation bottom associated with a horizontal displacement at the lower extremity of the wall (excavation side).

Overall it is observed that the shapes of the wall deflection are well predicted by the numerical model, in particular regarding to the locations of maximum deflection.

The inclinometer which was installed inside the diaphragm wall is able to record only the relative displacements of the retaining wall, related to a point considered to be fixed (in this case the lower extremity of the inclinometer), while the numerical calculations show non-zero displacement at this level (horizontal displacement toward the excavation). Thus, to best compare the results of measurements and those from the numerical model, it is permissible to correct the measurements, and to make them as close as possible to the numerical model by modifying this value of zero. For this, an absolute value of the lateral displacements (appropriate to the computed displacement of the

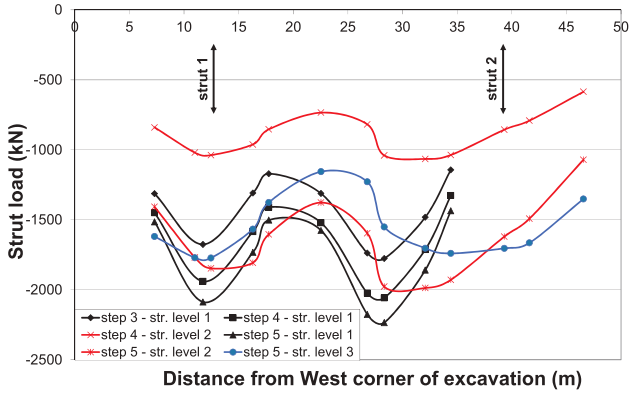

Fig. 20. Evolution of the axial forces in struts along the wall.

lower extremity) should be additionally considered to the horizontal displacement profile recorded by the inclinometers and displayed in Figs. 18 and 19. In turn, this shall lead to a better convergence of the computed displacements with the measured ones.

According to Figs. 18 and 19, it can be observed that the numerical results tend to overestimate slightly the inclinometer measurements in the calculation steps 2, 3 and 4. However, at the end of excavation works (after the 5th and 6th step), the results show close agreement between the finite difference analysis results and the field observations; both for the shape and magnitude of the displacement curves. The numerical model convergence at the final excavation stage can be partly explained by the fact that the measured displacements at this stage are larger than those obtained at intermediate phases, the effect of measurement uncertainties (constant over time, approximately ± 1 mm over a total height of 30 m) is relatively low.

3.3. Compression forces in struts

Fig. 20 shows the evolution of the axial force during the various phases of excavation in different struts along the wall. From this figure it is observed that the axial force regularly increases during the excavation. After the calculation steps 3, 4 and 5, there is a significant variation of the axial force in the struts along the excavation. Approaching the two corners (East and West) of the excavation or the salient part of the excavation wall, efforts in the struts decreases (due to the corner stiffening effects). In areas where the movement of the wall are maximal (as it was already observed in Fig. 17), efforts in the struts are also maximum. After the 5th calculation step (full excavation phase), there is a significant increase (approximately 70%) compared to the previous calculation step (step 4) of efforts in the struts of the second level. However, efforts in the struts of the first level increased by only 7.5%.

Fig. 21 summarizes the measured and calculated strut loads at the

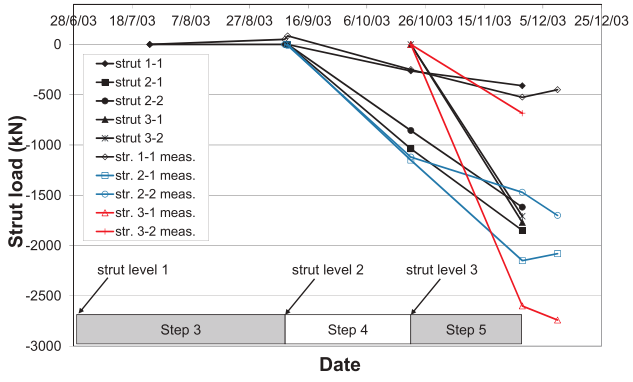

Fig. 21. Comparison of calculated (Flac^{3D}) and measured axial forces in struts.

end of Phases 3, 4 and 5. It is noted that the different excavation phases lead to an increase in struts load.

Comparing the calculated axial loads with the measured ones, it appears that the results are quite exploitable and very satisfactory for the upper and middle struts. The loads measured in these struts are on average close to the calculated values, with uncertainties closely related to the measuring mode and the temperature variation. Regarding the bottom struts, the calculated load in the strut 3-1 (at the position of the inclinometer I_1) is relatively comparable to measurements. However, the calculated effort in the strut 3-2 (location of the inclinometer I_2) is about 2 times larger than the value measured by the strain gauges. The difference noted in the strut 3-2 is probably due to measurement error. The axial loads measured in the struts 3-1 and 3-2 should be consistent because they are located in areas where the movement of the wall are also consistent (cf. Fig. 17). Otherwise, it was noted during the instrumentation that this strut was badly stalled and that it is only after a while that it begins to be compressed (Bonnet-Eymard et al. 2005).

Nevertheless, Fig. 21 shows that the forces calculated in the two struts of the third level (strut 3-1 and 3-2) are well framed by the measurement averages of efforts developed in these two struts after the complete excavation phase.

Otherwise, the 2D calculation revealed that loads are always larger than those predicted by the 3D model in a variable ratio with the phase and position of the struts. For the final excavation phase, a difference of 18%, 38% and 50% was observed for the upper, middle and bottom struts, respectively.

3.4. Impact on surface adjacent structures

The impact on adjacent structures is estimated through the monitoring of a one-storey brick building *A* (Section 1 - see Fig. 1). The analysis first concentrates on surface settlements along the West side of the instrumented building (points I_{11} to I_{17}, cf. Fig. 1) and on Greenfield settlements (leveling surface points I_{21} to I_{27}, Section 2) and focuses then on horizontal deformations of this building.

3.4.1. Ground surface settlements

The geometric, structural and mechanical characteristics of existing buildings are not precisely known, in particular the structural elements and foundations (although it also known that these are shallow). In this case, due to this lack of precise information, a simple model was used to represent the instrumented building with Flac^{3D}. This building was modeled by concrete solid elements (14 layers of solid elements). It results from a parametric analysis of the influence of the discretisation of the building on the quality of the results that it is necessary to have a refined mesh in the building thickness to obtain precise results of the surface settlement. Parametric analysis showed that surface settlement profiles converge using a number of layers slightly lower than that finally considered.

The surface settlement troughs calculated on the greenfield transverse profile (from I_{21} to I_{27}) and along the East side of the instrumented building (from I_{33} to I_{37}) at each phase of excavation are presented in Figs. 22 and 23, respectively. In the same figures the field measurements at the end of excavation are also presented.

It is noticed from figures that the 3D numerical analysis clearly shows a settlement profile of concave type, with increasing amplitude with the depth of excavation. This settlement type is consistent with the deep inward profiles of the wall deflection observed in Figs. 18 and 19.

At the final excavation phase, the maximum settlement δ_{vm} reached below the brick building is about 3.1 mm (against 2.7 mm in Greenfield conditions) and is obtained at 13.5 m from the top of the wall. This horizontal distance from the wall is close to 0.8% of the excavation depth (instead 0.7% in greenfield).

The amplitude of the ground surface settlements is lower than that of the lateral displacements of the wall. The deformation ratio between the maximum settlement δ_{vm} and the associated maximum horizontal

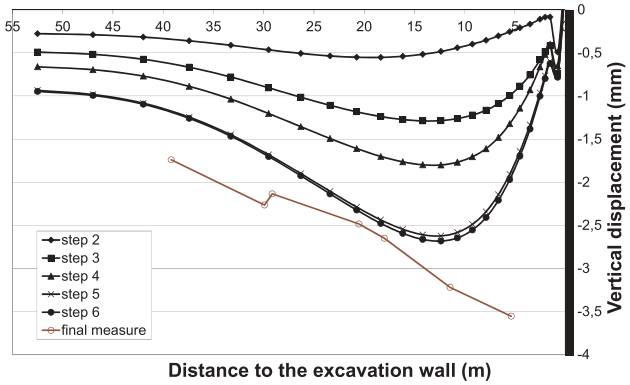

Fig. 22. Greenfield calculated settlement trough.

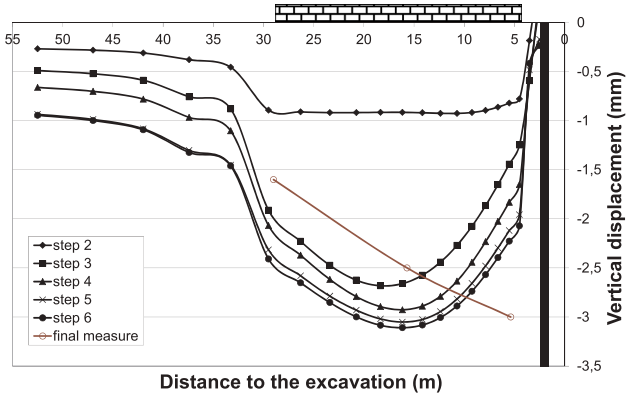

Fig. 23. Settlement trough calculated on the east side of the building *A*.

displacement δ_{hm} is close to 0.3.This corresponds to low values compared to the range of 0.5 to 2 given by Clough and O'Rourke (1990), Ou et al. (1993), Moormann (2004), Leung and Ng (2007) and Capraru and Adam (2014). This aspect could be partly explained by the overconsolidated behavior of the Toulouse's molasses and by the high value of K_0 coefficient.

In terms of magnitude of maximum surface settlements at the end of works, calculated results and in situ measurements are in good agreement. It is noteworthy that unlike the measures for the western facade of the building, the numerical analysis does not provide the fast decrease measured in the settlements of the north side of the building (the farthest from the top of the wall). However, in greenfield conditions numerical calculation predicts a relatively significant decrease in the same manner as the measurements.

3.4.2. Horizontal deformations

Fig. 24 presents the evolution of horizontal deformations on the west side of the instrumented building *A* during the excavation works. The horizontal deformation ε_h between two points is calculated analogously to the real measurement as the difference between the horizontal displacements of these two points divided by the corresponding horizontal distance. It is represented midway between the two points. A positive value means a horizontal distance increase.

Fig. 24 shows that an extension is developed along the facade from the first phase of work. This extension does not cease to progress with the depth of excavation in the zone furthest away from the wall. According to Fig. 24, it can be observed overall that the calculated horizontal extensions seem underestimated compared to measurements. The total increase of calculated distance between points I_{11} and I_{17} is about 3.5 mm at the end of stage 6 (against a measured increase of 8.6 mm). At the same time, Fig. 18 shows that the deflection of the top of the wall is close to 3.9 mm. Thus, the wall horizontal displacements

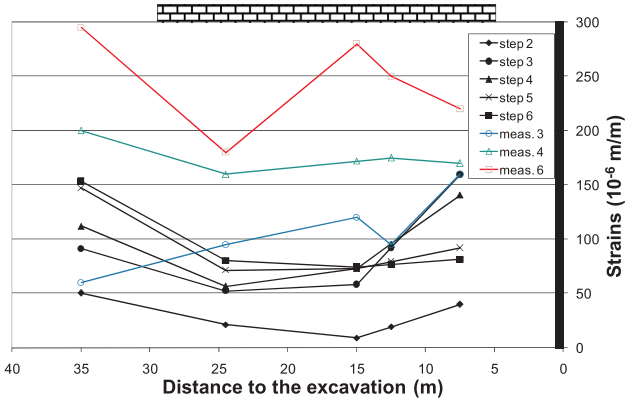

Fig. 24. Comparison of calculated and measured horizontal extension.

agree well with the total increase of horizontal distance behind the wall. Since the horizontal displacement at the top of the wall from 3D analysis are very close to the field measurements at the final stage of excavation, the difference observed between the calculated and measured horizontal deformations can be partly explained by measurements errors of horizontal extension measuring devices.

4. Conclusions

The full set of experimental results, obtained during the excavation of the 17.2 m deep Saint-Agne subway station, provided an opportunity for validating numerical models. Design analyses, needed to investigate all critical aspects of soil-structure interaction and construction sequences, have been performed using a full 3D finite differences model (the 2D analysis is inaccurate due to the corner stiffening and geometrical effects). Based on results of the field observations and analysis presented herein, the following conclusions can be drawn:

- The observed displacements and settlements remain rather limited (compared to the values specified in the literature). Possible explanations of these results include the improvement of the construction techniques, the number of struts (and their characteristics) used in this particular case study but also the good mechanical properties of the Toulouse molasses. It appears that, even though the data include very different physical or mechanical parameters (wall deflection, strut load, settlement, horizontal extension and crack opening), there is a global consistency of these results.
- The horizontal and vertical movements around the excavation wall showed an atypical deformation scheme, the maximum horizontal displacements of the wall being triple the maximum ground surface settlements. The high initial K_0 value and the highly overconsolidated character of the Toulouse molasses seem to be responsible for larger than expected horizontal movements.
- Both the 3D and 2D analyses cannot fully match the field measurements, indicating that some factors, such as construction delay, over excavation, and temperature effects, are very difficult to account for in the analyses. Nonetheless, the lateral movements at final state were very well predicted by the 3D analysis, whereas the plane strain 2D analysis consistently overpredicts the maximum wall deflection by about 30%. This suggests that some corner constraint effects persist and plane strain conditions do not completely prevail even at the midspan sections of this excavation.
- At the end of the excavation the maximum recorded settlement behind the wall is also well reproduced by the 3D numerical model. However, unlike measurements, the description of the pattern of the settlement trough remains inadequate. This difference may be related to a conservative estimate of the stiffness of the building and may depend on the constitutive model of the soil. It should be remembered that the used constitutive model does not take into

account the nonlinear behavior at small strains.

- Using a soil behavior model with simple failure criteria, such as Mohr-Coulomb, which takes into account a Young's modulus that increases linearly with the depth, allowed to properly simulate the behavior of the excavation and to obtain an acceptable agreement between the numerical results and the measurements for all phases of work.

In addition, the following recommendations and precautions can be drawn:

- It should be noted that the operational stiffness of the passive struts (axial stiffness under working conditions) is often much lower than the nominal stiffness adopted during the design process, due in part to the inevitable bending forces and the rarely ideal support conditions that introduce additional deformations. Therefore, in any numerical analyses for design purposes and for prediction of the performance of deep excavations, it is necessary to choose appropriate values for the operational stiffness parameters. In the current study, in all analysis the struts stiffness was reduced to 50% of its nominal value. The reduction value, however, might vary from one project to another.
- The diaphragm wall is unlikely to be a continuous membrane along the sides of the excavation, as it is constructed by sections of wall panels that are not fully connected in this direction. Consequently, it cannot sustain any significant out-of-plane bending, and the horizontal stiffness of the wall is also much smaller than the stiffness of the solid concrete. Therefore, to obtain realistic results in 3D analyses, the axial and bending stiffness of the wall along its perimeter must be reduced.
- The density of the mesh in zones near the diaphragm walls had major effect on the accuracy of 3D analysis. On the other hand, the mesh density in remote areas apparently had less significant effects on accuracy of numerical results. A refined mesh in zones close to the walls coupled with an appropriate number of mesh elements far away from the excavated area resulted in quick convergence in analysis. This finding greatly reduced the computation time, and therefore makes 3D analysis economically feasible.
- The relative displacements of each inclinometer casing are not enough to better understand the lateral soil movements; the displacement of the top of the inclinometer must also be measured by topographical device (automated total station) which allows to have an absolute reference of displacement and to correct all the measurements.
- If the estimated damage level is unacceptable, protective measures should be considered. These may include controlling construction procedures, changing construction methods, increasing support stiffness, improving the ground, or reinforcing foundations and structures.

The authors hope that the publication of this case study will help to stimulate further research into this aspect of deep excavation behavior.

Acknowledgement

The research project METROTOUL would not have been possible without the kind permission and constant support of the SMAT society. The authors would also like to thank for the financial support of METROTOUL research program the French Ministry of Research through the Network Civil Engineering and Urban (RGC& U). They finally would like to acknowledge the help of the different contractors in collecting data.

References

Bonnet-Eymard, T., Emeriault, F., Kastner, R., 2005. Toulouse subway line B: Auscultation-Instrumentation on station, Plot 5- Saint Agne Station, Report No. 6.
Briaud, J.L., Nicholson, P., Lee, J., 2000. Behaviour of a Full-Scale VERT Wall in Sand. ASCE J. Geotech. Geoenviron. Eng. 126 (9), 808–818.
Capraru, C., Adam, D., 2014. Evaluating the influence of deep excavations on neighbouring buildings by numerical analysis. In: Hicks (Ed.), Proceedings of the 8th European conference on Numerical Methods in Geotechnical Engineering. Taylor & Francis Group, Delft, pp. 729–734.
Caudron, M., 2007. Experimental and numerical study of the soil-structure interaction in the occurrence of a sinkhole. PhD thesis, INSA of Lyon, France (in French).
Clough, G.W., O'Rourke, J.M., 1990. Construction induced movementsinsitu walls. Proc Conf Design and performance of earth retraining. In: ASCE: Geotech. Spec Cornell University, New York, pp. 439–470.
Emeriault, F., Kastner, R., Vanoudheusden, E., 2008. Movements induced by tunneling with an EPB machine in overconsolidated soils: compans monitoring section of Toulouse subway line B. In: 6th international conference case histories in geotechnical engineering, Arlington, VA.
Finno, R.J., Blackburn, J.T., Roboski, J.F., 2007. Three-dimensional effects for supported excavations in clay. ASCE J. Geotech. Geoenviron. Eng. 133 (1), 30–36.
Franzius, J.N., Potts, D.M., Burland, J.B., 2006. The response of surface structures to tunnel construction. Proc. Inst. Civ. Eng. Geotech. Eng. 159 (1), 3–17.
Ghareh, S., Saidi, M., 2011. An investigation on the behavior of retaining structure of excavation wall using obtained result from numerical modeling and monitoring approach. J. Struct. Eng. Geotech. 1 (2), 17–23.
Hong, Y., Ng, C.W.W., Liu, G.B., Liu, T., 2015. Three-dimensional deformation behaviour of a multi-propped excavation at a "greenfield" site at Shanghai soft clay. Tunn. Undergr. Space Technol. 45, 249–259.
Houhou, M.N., Emeriault, F., Kastner, R., Benmebarek, S., 2010. Rétro-analyse tridimensionnelle d'une excavation profonde multi-supportée instrumentée. Eur. J. Environ. Civil Eng. 14 (1), 55–86.
Houhou, M.N., Emeriault, F., Vanoudheusden, E., 2016. Three-dimensional back-analysis of an instrumented shallow tunnel excavated by a conventional method. Geotech. Geol. Eng. 34 (4), 1101–1117.
Hsieh, P.G., Ou, C.Y., 1998. Shape of ground surface settlement profiles caused by excavation. Can. Geotech. J. 35, 1004–1017.
Itasca Consulting Group Inc FLAC3D Version 5, 2012.User's Guide. Minneapolis, Minnesota.
Leung, H.Y., Ng, C.W., 2007. Wall and ground movements associated with deep excavations supported by cast in situ wall in mixed ground conditions. ASCE J. Geotech. Geoenviron. Eng. 133 (2), 129–143.
Lin, D.G., Chung, T.C., Phien-wej, N., 2003. Quantitative evaluation of corner effect on deformation behavior of multi-strutted deep excavation in Bangkok subsoil. Geotech. Eng. 34 (1), 41–57.
Long, M., 2001. Database for retaining wall and ground movements due to deep excavations. ASCE J. Geotech. Geoenviron. Eng. 127 (3), 203–224.
Moormann, C., 2004. Analysis of wall and ground movements due to deep excavations in soft soil based on a new worldwide database.Soils. Foundations 44 (1), 87–98.
Ou, C.Y., Hsien, P.G., Chiou, D.C., 1993. Characteristics of ground surface settlement during excavation. Can. Geotech. J. 30, 758–767.
Ou, C.Y., Liao, J.T., Cheng, W.L., 2000. Building response and ground movements induced by a deep excavation. Geotechnique 50 (3), 209–220.
Peck, R.B., 1969. In: Proceedings of the 7th International Congress of Soil Mechanics and Foundation Engineering, pp. 225–285.
Schweiger, H.F., 2008. The role of advanced constitutive models in geotechnical engineering. GeomechanikundTunnelbau 1 (5), 336–344.
Serratrice, J.F, 2005.Toulouse subway line B: Laboratory tests. Report n° 22546-01, CETE d'Aix.
Shao, Y., Macari, E.J., 2008. Information feedback analysis in deep excavations. Int. J. Geomech. 8 (1), 91–101.
Son, M., Cording, J., 2005. Estimation of building damage due to excavation-induced ground movements. ASCE J. Geotech. Geoenviron. Eng. 131 (2), 162–177.
Wang, J.H., Xu, Z.H., Wang, W.D., 2010. Wall and ground movements due to deep excavations in Shanghai soft soils. ASCE J. Geotech. Geoenviron. Eng. 136 (7), 985–994.
Zdravkovic, L., Potts, D.M., St John, H.D., 2005. Modelling of a 3D excavation in finite element analysis. Geotechnique 55 (7), 497–513.